

Model Hierarchy Predictive Control of Robotic Systems

He Li, Robert J. Frei, Patrick M. Wensing

Abstract—This paper presents a new predictive control architecture for high-dimensional robotic systems. As opposed to a conventional Model-Predictive Control (MPC) approach that formulates a hierarchy of optimization problems, the proposed work formulates a single optimization problem posed over a hierarchy of models, and is thus named Model Hierarchy Predictive Control (MHPC). MHPC is formulated as a multi-phase receding-horizon Trajectory Optimization (TO) problem, and is solved by an efficient solver called Hybrid Systems Differential Dynamic Programming (HSDDP). MHPC is benchmarked in simulation on a quadruped, a biped, and a quadrotor, demonstrating control performance on par or exceeding whole-body MPC while maintaining a lower computational cost in each case. A preliminary bounding experiment is conducted on the MIT Mini Cheetah with the control policy generated offline, demonstrating the physical validity of the generated trajectories and motivating online MHPC in future work.

I. INTRODUCTION

Whether for agriculture, construction, or disaster response, the mobility afforded by legs offers promise for future robots that can go where we go. Despite rapid progress in the past decade toward this vision, the operational envelope of existing legged robots remains limited. Time-consuming tuning in the lab is usually necessary for every new behavior and every new robot. While this approach may be acceptable for current robots to operate in known scenarios, future robots must master the ability to generate stable motion on the fly to succeed in navigating novel real-world environments.

Model Predictive Control (MPC) is a powerful tool in optimal control and has been gaining popularity in the legged robot community over the past decade [1]–[5]. Compared to conventional optimal control methods such as the Linear Quadratic Regulator (LQR), MPC considers system dynamics as well as various constraints, e.g., control limits and path constraints. MPC repeatedly solves a finite-horizon trajectory optimization (TO) problem from the current state. The first control signal is executed and the next state is measured. The TO is then resolved with the new current state. The performance of MPC depends on the dynamics model used, horizon length, and update frequency. This work proposes a new MPC configuration by using hierarchical model structures over the planning horizon to accelerate the solution of these problems.

Current MPC for legged robots mainly takes two approaches, the conventional reduced-order MPC (simple-model MPC) and whole-body MPC. Simple-model MPC formulates a hierarchy of optimization problems. This is done by generating a long-term low-dimensional plan based

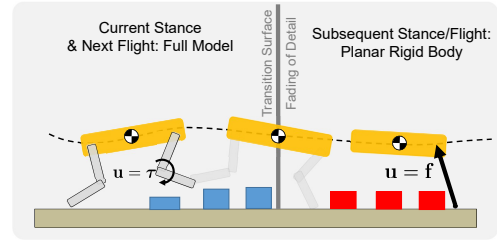


Fig. 1: Concept vision of MHPC for a quadruped navigating obstacles. MHPC uses multiple models over the planning horizon to capture performance benefits of whole-body MPC with the computational benefits of simple-model planning.

on a simple model, then solving a quadratic optimization (QP) problem instantly based on the full model to track the plan. Commonly used simple models include the Linear Inverted Pendulum Model (LIP) [2], [6], Spring-Loaded Inverted Pendulum Model (SLIP) [4], [7], and Single-Rigid-Body Model [3], [8], [9]. Centroidal dynamics models have also been used that consider the linear and angular momentum of the system as a whole [10]–[14]. MPC with simple models has the advantage of fast computation and not relying heavily on a warm start. However, meticulous tuning is typically required since heuristics are often used on top of MPC. Further, there is a complex interplay between short-term constraints posed within a QP and other long-term constraints, which may also lead to a time-consuming tuning process. In addition, the operational envelope of the resulting motions from simple models is limited. For example, motions such as climbing stairs could not be generated with a LIP model since it normally neglects all kinematics constraints and assumes constant height and zero angular momentum.

By comparison, whole-body MPC can generate more complex behaviors by considering the full range of possible motions. As opposed to simple-model MPC where the control is computed instantly, whole-body MPC finds a sequence of torque commands by solving a finite-horizon TO problem that ensures long-term balance, enabling recovery from larger disturbances. Despite these benefits, the *curse of dimensionality* from the high-dimensional dynamics of legged robots has prevented it from being popular, and the underlying TO problem can be highly non-convex, requiring a good initial guess. Recent results (e.g., [1]) using Differential Dynamic Programming (DDP) [15] have shown great promise for online use of whole-body MPC. Since then, many DDP advances have been proposed, demonstrating real-time performance in simulation [16]–[18] and on hardware [5], [19]. Though some of these works could solve a whole-body TO problem for a quadruped, computational requirements are still significantly greater than for simple-model MPC. Hardware implementations to date do not demonstrate agile maneuvers, as these motions are further

*This work was supported by NSF Grant CMMI-1835186 and ONR Award N0001420WX01278.

Authors are with Department of Aerospace and Mechanical Engineering, University of Notre Dame, Notre Dame, IN 46556 USA (hli25@nd.edu, rfrei@nd.edu, pwensing@nd.edu)

hindered by computational challenges.

A. Contribution

The major contribution of this research is to propose Model Hierarchy Predictive Control (MHPC), a new method that carries out planning within MPC based on a hierarchy of models over the planning horizon. Overall, MHPC is shown to unify the computational and performance benefits of simple-model MPC and whole-body MPC. Figure 1 conceptually illustrates the main idea of MHPC with a planar quadruped that needs to account for obstacles when planning its movement. In the current stance and next flight, the robot coordinates its legs and whole-body dynamics to avoid the blue obstacles and to balance itself. Since the subsequent stance and flight are far away, it strategically ignores leg details and instead only considers how its body should move to navigate the rest of the terrain. In this way, the quadruped focuses on its near-term balance while having a rough plan in mind for the long term. This work makes a first step toward this goal by studying the underlying mechanism, i.e., carrying out MPC with planning over a hierarchy of models.

The rest of this paper is structured as follows. Section II discusses the main idea of MHPC and formulates the MHPC problem mathematically. An efficient DDP-based solver is introduced for MHPC as well. Section III presents a hierarchy of models for three example systems. The performance of MHPC is then benchmarked in simulation in Section IV. In Section V, we run MHPC offline and execute the control policy in a dynamics simulator and on hardware. Section VI concludes the paper and discusses future work.

II. MODEL HIERARCHY PREDICTIVE CONTROL

In this section, we further describe the main idea of MHPC. Compared to simple-model MPC, which formulates a hierarchy of optimization problems, MHPC constructs a single optimization problem posed over a hierarchy of models. Main differences are conceptually shown in Fig. 2. MHPC plans with full-model dynamics in near term and with an abstract simple model in the long term. The consistency between the two is enforced by a low-dimensional transition constraint. Due to the reduced dimensionality of the simple model, this transition typically incorporates a projection map. Figure 2 incorporates only two model hierarchies, but, in general, MHPC can use multiple models and regards the

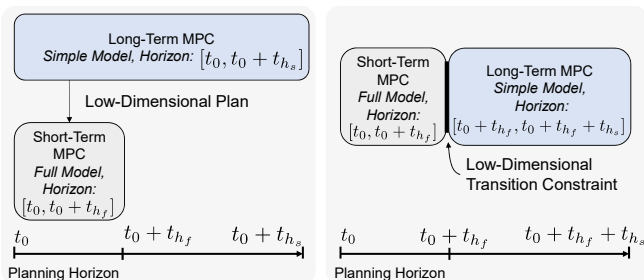


Fig. 2: Novelty of MHPC compared to conventional MPC. Left: Simple-model MPC formulates a hierarchy of optimization problems. Right: MHPC constructs a single optimization problem over a hierarchy of models.

higher-order model as a ‘full model’ and the lower-order model as a ‘simple model’.

At the core of MHPC is an abstraction schedule specifying the planning horizons for each model. In Fig. 2, t_{h_f} and t_{h_s} respectively represent planning horizons for a full model and a simple model. The abstraction schedule affects MHPC performance in terms of disturbance rejection and computational cost. Planning based exclusively on the full model and exclusively on a simple model represent two extremes of how to configure MHPC. In this work, we discuss these effects for several example systems in Section III.

A. Problem Formulation

MHPC can be formulated as a multi-phase receding-horizon TO problem. A system with multi-phase dynamics can be modeled as follows:

$$\mathbf{x}_{k+1}^{[i]} = \mathbf{f}_i(\mathbf{x}_k^{[i]}, \mathbf{u}_k^{[i]}), \quad (1a)$$

$$\mathbf{x}_0^{[i+1]} = \mathbf{P}_i(\mathbf{x}_{N_i}^{[i]}), \quad (1b)$$

$$g_i(\mathbf{x}_{N_i}^{[i]}) = 0, \quad (1c)$$

where \mathbf{x} and \mathbf{u} are system state and control vectors, i denotes the phase index, k the time index, \mathbf{f} gives the dynamics evolution, and \mathbf{P} represents phase transition map. The state and control vectors may have a different dimension in each phase. Note that \mathbf{f} is in discrete time and is obtained via a numerical integration scheme, with forward Euler used in this work. Other integration schemes can be used without loss of generality to the remaining development. The equation (1c) specifies a transition constraint under \mathbf{P}_i .

We alert the readers that the formulation (1) is a generalization of other hybrid systems models commonly used in legged locomotion work (e.g., [20]) where the transition map normally accounts for impacts. In (1), \mathbf{f} may specify the dynamics for a phase of the full model (e.g., stance dynamics or flight dynamics of a full quadruped) or of a simple model. The transition map \mathbf{P} may thus describe a reset map at impact, as well as a transition that maps the state of the full model to the state of a simpler model, as captured by the transition constraint in Fig. 2. For example, when working with the SLIP model, the transition map could account for the impact in the full model and then extract the CoM state post-impact as the initial condition for the SLIP.

For each phase i of (1), we define a cost function

$$J^{[i]}(\mathbf{x}_0^{[i]}, \mathbf{U}^{[i]}) = \sum_{k=0}^{N_i-1} \ell_i(\mathbf{x}_k^{[i]}, \mathbf{u}_k^{[i]}) + \phi_i(\mathbf{x}_{N_i}^{[i]}), \quad (2)$$

where ℓ_i , ϕ_i and N_i represent the running cost, the terminal cost, and the length of horizon, respectively, associated with phase i , and $\mathbf{U}^{[i]} = [\mathbf{u}_0^{[i]}, \dots, \mathbf{u}_{N_i-1}^{[i]}]$. For a system (1) with n phases, the TO problem can be formulated as follows

$$\min_{\mathbf{u}} \sum_{i=1}^n J^{[i]}(\mathbf{x}_0^{[i]}, \mathbf{U}^{[i]}) \quad (3a)$$

$$\text{subject to } (1a), (1b), \quad (3b)$$

$$(1c), \quad (3c)$$

$$h_i(\mathbf{x}_k^{[i]}, \mathbf{u}_k^{[i]}) \geq 0, \quad (3d)$$

where $\mathcal{U} = [\mathbf{U}^{[1]}, \dots, \mathbf{U}^{[n]}]$ and h represent inequality constraints such as torque limits and friction constraints. Solving (3) with receding horizons then gives rise to MHPC.

B. Hybrid Systems Solver for MHPC

We employ an efficient algorithm, Hybrid Systems Differential Dynamic Programming (HSDDP), developed in [18], to solve the multi-phase optimization problem (3). HSDDP attacks (3) by converting it into an unconstrained optimization problem using Augmented Lagrangian (AL) [21], [22] and Reduced Barrier (ReB) methods. A Lagrangian-like function for phase i is constructed as follows

$$\begin{aligned} \mathcal{L}^{[i]}(\mathbf{x}_0^{[i]}, \mathbf{U}^{[i]}, \lambda_i, \sigma_i, \delta_i) = & \sum_{k=0}^{N_i-1} \underbrace{\ell_i(\mathbf{x}_k^{[i]}, \mathbf{u}_k^{[i]}) + B_{\delta_i}(h_i(\mathbf{x}_k^{[i]}, \mathbf{u}_k^{[i]}))}_{L_i(\mathbf{x}_k^{[i]}, \mathbf{u}_k^{[i]})} \\ & + \underbrace{\phi_i(\mathbf{x}_{N_i}^{[i]}) + \left(\frac{\sigma_i}{2}\right)^2 g_i(\mathbf{x}_{N_i}^{[i]}) + \lambda_i g_i^2(\mathbf{x}_{N_i}^{[i]})}_{\Phi_i(\mathbf{x}_{N_i}^{[i]})}, \end{aligned} \quad (4)$$

where λ_i and σ_i are the Lagrange multiplier and penalty coefficient, respectively, and B_{δ_i} is a reduced Barrier function [18], [23] with relaxation parameter δ_i . The Lagrangian-like function for the entire multi-phase system (1) is then

$$\mathcal{L}(\mathcal{U}, \lambda, \sigma, \delta) = \sum_{i=1}^n \mathcal{L}^{[i]}(\mathbf{x}_0^{[i]}, \mathbf{U}^{[i]}, \lambda_i, \sigma_i, \delta_i), \quad (5)$$

where $\lambda = [\lambda_1, \dots, \lambda_n]$, σ and δ are similarly defined.

The reformulated unconstrained problem is then:

$$\min_{\mathcal{U}} \mathcal{L}(\mathcal{U}, \lambda, \sigma, \delta) \quad (6a)$$

$$\text{subject to (1a), (1b).} \quad (6b)$$

HSDDP solves (6) with fixed λ, σ, δ using DDP, and employs an outer loop to iteratively reset their values until all constraints are satisfied. The update equations are as follows

$$\sigma \leftarrow \beta_\sigma \sigma, \quad \lambda \leftarrow \lambda + \sigma \circ \mathbf{g}, \quad \delta \leftarrow \beta_\delta \delta, \quad (7)$$

where $\beta_\sigma > 0$ and $0 < \beta_\delta < 1$ are update parameters, the vector $\mathbf{g} \in \mathbb{R}^n$ concatenates $g_i(\mathbf{x}_{N_i}^{[i]}) \forall i = 1, \dots, n$, and the operator \circ denotes element-wise product.

Care must be taken when solving (6) with DDP due to the discontinuous jump (for hybrid systems) or state projection (for model transition) caused by (1b). This is addressed in HSDDP by employing an impact-aware step. Denote $V(\mathbf{x}_k^{[i]})$ the optimal cost-to-go evaluated at $\mathbf{x}_k^{[i]}$. The variation of $V(\mathbf{x}_k^{[i]})$ along a nominal trajectory under perturbation $(\delta \mathbf{x}_k^{[i]}, \delta \mathbf{u}_k^{[i]})$ is approximated to the second order as follows

$$\delta V(\delta \mathbf{x}_k^{[i]}) \approx \frac{1}{2} (\delta \mathbf{x}_k^{[i]})^\top \mathbf{S}_k^{[i]} \delta \mathbf{x}_k^{[i]} + (\mathbf{s}_k^{[i]})^\top \delta \mathbf{x}_k^{[i]} + s_k^{[i]}, \quad (8)$$

where $\mathbf{S}_k^{[i]}$, $\mathbf{s}_k^{[i]}$, and $s_k^{[i]}$ respectively, represent the Hessian, gradient, and scalar terms. HSDDP recursively computes

Algorithm 1 HSDDP Algorithm

- 1: Initialize λ, σ, δ .
 - 2: **while** $\|\mathbf{g}\|_2 > \text{tol}$. **do**
 - 3: Minimize $\mathcal{L}(\mathcal{U}, \lambda, \sigma, \delta)$ using DDP (carry out Eq. (11) at mode transition in backward sweep).
 - 4: Compute $g_{c_i}(\mathbf{x}_{N_i}^{[i]})$.
 - 5: Update λ, σ, δ using Eq. (7)
 - 6: **end while**
-

these terms for all k and i by performing a backward sweep. For $0 \leq k < N_i$ in phase i , the recursive equations are [1]

$$s = s' + \frac{1}{2} Q_{\mathbf{u}}^T Q_{\mathbf{uu}}^{-1} Q_{\mathbf{u}}, \quad (9a)$$

$$\mathbf{s} = Q_{\mathbf{x}} - Q_{\mathbf{ux}}^T Q_{\mathbf{uu}}^{-1} Q_{\mathbf{u}}, \quad (9b)$$

$$\mathbf{S} = Q_{\mathbf{xx}} - Q_{\mathbf{ux}}^T Q_{\mathbf{uu}}^{-1} Q_{\mathbf{ux}}, \quad (9c)$$

where

$$Q_{\mathbf{x}} = \mathbf{L}_{\mathbf{x}} + \mathbf{f}_{\mathbf{x}}^\top \mathbf{s}', \quad (10a)$$

$$Q_{\mathbf{u}} = \mathbf{L}_{\mathbf{u}} + \mathbf{f}_{\mathbf{u}}^\top \mathbf{s}', \quad (10b)$$

$$Q_{\mathbf{xx}} = \mathbf{L}_{\mathbf{xx}} + \mathbf{f}_{\mathbf{x}}^\top \mathbf{S}' \mathbf{f}_{\mathbf{x}} + \mathbf{s}' \cdot \mathbf{f}_{\mathbf{xx}}, \quad (10c)$$

$$Q_{\mathbf{uu}} = \mathbf{L}_{\mathbf{uu}} + \mathbf{f}_{\mathbf{u}}^\top \mathbf{S}' \mathbf{f}_{\mathbf{u}} + \mathbf{s}' \cdot \mathbf{f}_{\mathbf{uu}}, \quad (10d)$$

$$Q_{\mathbf{ux}} = \mathbf{L}_{\mathbf{ux}} + \mathbf{f}_{\mathbf{u}}^\top \mathbf{S}' \mathbf{f}_{\mathbf{x}} + \mathbf{s}' \cdot \mathbf{f}_{\mathbf{ux}}, \quad (10e)$$

in which subscripts indicate partial derivatives and the prime indicates the next time step. Note that $\mathbf{f}_{\mathbf{xx}}$, $\mathbf{f}_{\mathbf{uu}}$ and $\mathbf{f}_{\mathbf{ux}}$ are tensors. The notation ' \cdot ' denotes matrix-tensor multiplication. At $k = N_i$ of phase i , the update equations are

$$s = s', \quad (11a)$$

$$\mathbf{s} = \Phi_{\mathbf{x}} + \mathbf{P}_{\mathbf{x}}^\top \mathbf{s}', \quad (11b)$$

$$\mathbf{S} = \Phi_{\mathbf{xx}} + \mathbf{P}_{\mathbf{x}}^\top \mathbf{S}' \mathbf{P}_{\mathbf{x}}. \quad (11c)$$

Note that in (11), the prime indicates the next step at $k = 0$ of phase $i + 1$. The value function approximation thus obtained is used to construct the control policy

$$\delta \mathbf{u}^* = -Q_{\mathbf{uu}}^{-1} (Q_{\mathbf{u}} + Q_{\mathbf{ux}} \delta \mathbf{x}) \equiv \boldsymbol{\kappa} + \mathbf{K} \delta \mathbf{x}. \quad (12)$$

A line search method and a regularization step are typically performed with (12) to ensure cost reduction [1]. Pseudo code for HSDDP is shown in Algorithm 1. The reader is referred to [18] for a detailed description.

Extending the horizon of a finite-horizon OCP helps to maintain long-term stability at the expense of additional computation. For example, the whole-body QP designed in [24] adds long-term balance constraints for a humanoid robot such that its state remains viable. Another approach is to embed future information into the terminal cost. An ideal terminal cost would be the value function of an infinite-horizon OCP, which, however, does not have an analytical solution in general and needs to be approximated. In this work, by planning over the long term with a simple model, MHPC provides a proxy of the value function for the full model to improve its long-term stability.

III. HIERARCHY OF MODELS AND ABSTRACTION SCHEDULES FOR EXAMPLE SYSTEMS

This section presents model hierarchies and defines transitions between the models for MHPC of a planar quadruped, a five-link biped, and a quadrotor.

A. Planar quadruped

The dynamics of a planar quadruped are hybrid since it frequently makes and breaks contact with ground. As a result, the full model of a quadruped could be described by system (1) whose dynamics are obtained as [16], [18]

$$\begin{bmatrix} \mathbf{H} & -\mathbf{J}_c^\top \\ -\mathbf{J}_c & \mathbf{0} \end{bmatrix} \begin{bmatrix} \ddot{\mathbf{q}} \\ \lambda_c \end{bmatrix} = \begin{bmatrix} \mathbf{S}^\top \boldsymbol{\tau} - \mathbf{C}\dot{\mathbf{q}} - \boldsymbol{\tau}_g \\ \mathbf{J}_c \dot{\mathbf{q}} \end{bmatrix}, \quad (13)$$

where $\mathbf{q} = [\mathbf{c}^\top, \theta, \mathbf{q}_{\text{joint}}^\top]^\top$ is the generalized coordinate, and $\mathbf{c} \in \mathbb{R}^2$, $\theta \in \mathbb{R}$, and $\mathbf{q}_{\text{joint}} \in \mathbb{R}^4$ denote the trunk center of mass (CoM), trunk orientation, and joint angles, respectively, and \mathbf{H} , $\mathbf{C}\dot{\mathbf{q}}$, $\boldsymbol{\tau}_g$, \mathbf{S} , and $\boldsymbol{\tau} \in \mathbb{R}^4$ denote the inertia matrix, Coriolis force, gravity force, selection matrix, and actuation torque, respectively. \mathbf{J}_c and λ_c represent the contact Jacobian and contact force, respectively, and their expressions depend on which foot is in contact with ground. During a flight mode, the matrix on the left side of (13) degenerates to the inertia matrix \mathbf{H} . Denoting $\mathbf{x}_f = [\mathbf{q}^\top, \dot{\mathbf{q}}^\top]^\top$ as the full model state, the state-space representation of (13) can then readily be obtained into the form (1). The reset map at touchdown is modeled considering impact dynamics as follows

$$\mathbf{P}_{\text{TD}}(\mathbf{x}^-) = \begin{bmatrix} \mathbf{I} & \mathbf{0} \\ \mathbf{0} & \mathbf{I} - \mathbf{H}^{-1} \mathbf{J}_c^\top (\mathbf{J}_c \mathbf{H}^{-1} \mathbf{J}_c^\top)^{-1} \mathbf{J}_c \end{bmatrix} \mathbf{x}^-, \quad (14)$$

where the superscript ‘-’ indicates the moment immediately before contact. The reset map at liftoff is smooth and simply is $\mathbf{P}_{\text{LO}}(\mathbf{x}^-) = \mathbf{x}^-$, where ‘-’ indicates the moment immediately before breaking contact.

For a quadruped robot, the weight of its legs is typically a fraction of its total weight. As result, a common simple model ignores the legs and considers only the trunk dynamics [3], [8], [9], [25] (Fig. 3). This model is described as follows

$$\begin{aligned} \ddot{\mathbf{c}} &= \frac{\mathbf{f}}{m} - \mathbf{g} \\ I\ddot{\theta} &= (\mathbf{p} - \mathbf{c}) \times \mathbf{f}, \end{aligned} \quad (15)$$

where \mathbf{c} , θ , and I represent the position of the CoM, the trunk orientation, and the body inertia, respectively. \mathbf{f} , \mathbf{g}

and \mathbf{p} denote the ground reaction force (GRF), gravitational acceleration, and the foot location, respectively. We denote $\mathbf{x}_s = [\mathbf{c}, \theta, \dot{\mathbf{c}}, \dot{\theta}]$ as the trunk model state. A projection map (Section I-A) is then defined such that $\mathbf{x}_s = \mathbf{T}\mathbf{x}_f$ where

$$\mathbf{T} = \begin{bmatrix} \mathbf{I}^3 & \mathbf{0}^{3 \times 4} & \mathbf{0}^{3 \times 3} & \mathbf{0}^{3 \times 4} \\ \mathbf{0}^{3 \times 3} & \mathbf{0}^{3 \times 4} & \mathbf{I}^3 & \mathbf{0}^{3 \times 4} \end{bmatrix} \quad (16)$$

and $\mathbf{I}^3 \in \mathbb{R}^{3 \times 3}$ is an identity matrix.

Quadruped bounding periodically executes four gait modes of motions: a back stance mode with the back foot on the ground, a flight mode, a front stance mode with the front foot on the ground, and another flight mode. Figure 3 illustrates an abstraction schedule used for quadruped bounding, which assigns the first two modes for the full model (13), (14), and the subsequent two modes for the trunk model (15). At the instant of touchdown shown in Fig. 3(a), a transition from full model to trunk model takes place. The low-dimensional transition thus considers the impact discontinuity (14) caused by touchdown, as well as the projection map (16), which is defined as follows

$$\mathbf{P}_2(\mathbf{x}_{N_2}^{[2]}) = \mathbf{T}\mathbf{P}_{\text{TD}}(\mathbf{x}_{N_2}^{[2]}). \quad (17)$$

In this context, the function $g_2(\mathbf{x}_{N_2}^{[2]})$ in (1) measures the vertical distance between the contact foot and ground, ensuring that touchdown occurs on the ground. The value function propagation (11) across the low-dimensional transition is then

$$\mathbf{s} = \Phi_{\mathbf{x}} + \frac{\partial \mathbf{P}_{\text{TD}}}{\partial \mathbf{x}}^\top \mathbf{T}^\top \mathbf{s}', \quad (18a)$$

$$\mathbf{S} = \Phi_{\mathbf{xx}} + \frac{\partial \mathbf{P}_{\text{TD}}}{\partial \mathbf{x}}^\top \mathbf{T}^\top \mathbf{S}' \mathbf{T} \frac{\partial \mathbf{P}_{\text{TD}}}{\partial \mathbf{x}}, \quad (18b)$$

where here the prime indicates the next step when the simple model starts. The equation (18) reveals that the trunk model is effectively used to set a terminal cost for the full model via a low-rank approximation, thus biasing the full model planning and reducing its dependence on a warm start.

We emphasize that the transition (17) is particular to the abstraction schedule at the time instant in Fig. 3(a). Since the optimization window is shifting as MHPC proceeds, this transition constraint changes as well. For example, if we shift the overall planning horizon one gait mode to the future, the transition would occur at takeoff and would be described by $\mathbf{P}_2(\mathbf{x}_{N_2}^{[2]}) = \mathbf{T}\mathbf{x}_{N_2}^{[2]}$. Further, the abstraction schedule assigns two gait modes to each model, whereas in general it could be varied to acquire high performance. This prospect is explored further in Section IV.

B. Five-link biped

A five-link biped robot is topologically equivalent to a planar quadruped (Fig. 3) except that its front and back legs are both pinned below the trunk CoM. Consequently, the full model (13) and (14), the simple model (15), and the abstraction schedule from Section III-A for quadruped bounding are also applied to biped running.

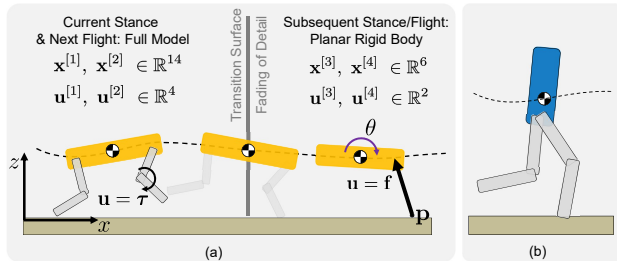


Fig. 3: Hierarchy of models for five-link robots with MHPC. (a) detailed abstraction schedule for planar quadruped bounding (b) the same abstraction is applied for biped running.

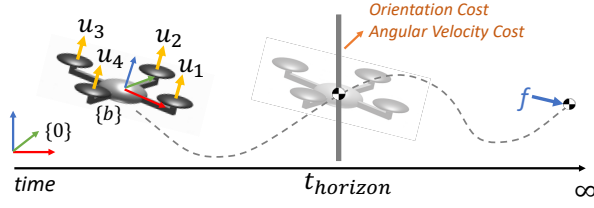


Fig. 4: Quadrotor followed by a point-mass template over the horizon.

C. Quadrotor

The last example explores the applicability of MHPC beyond legged robots. The dynamics of a quadrotor are underactuated, with thrust from the rotors only providing force in one direction, and body torques rigidly coupled to thrusts. The quadrotor (Fig. 4) is modelled as a rigid body with four thrust inputs, each at a moment arm r from the CoM. The acceleration of the quadrotor CoM is modelled as

$${}^b\mathbf{a} = \frac{1}{m} \begin{bmatrix} 0 \\ 0 \\ u_1 + u_2 + u_3 + u_4 \end{bmatrix} + {}^b\mathbf{R}_0^0 \mathbf{g} \quad (19)$$

with its rotational dynamics modelled as

$${}^b\bar{\mathbf{I}}^b \dot{\boldsymbol{\omega}} + {}^b\boldsymbol{\omega} \times {}^b\bar{\mathbf{I}}^b \boldsymbol{\omega} = \begin{bmatrix} r(u_2 - u_4) \\ r(u_3 - u_1) \\ k_m(u_1 + u_3 - u_2 - u_4) \end{bmatrix},$$

where the effort vector $\mathbf{u} = [u_1, u_2, u_3, u_4]^T$ contains the linear thrust of each rotor, ${}^b\bar{\mathbf{I}} \in \mathbb{R}^{3 \times 3}$ is the Cartesian inertia of the drone about its CoM, m its mass, and ${}^b\boldsymbol{\omega}$ its rotational velocity. In all cases, the pre-superscript indicates the frame that is used to express each vector. To approximate the yaw torque provided by the inertia of the counter rotating blades, k_m is used as a ratio of the difference in thrust from the blades and the moment applied on the drone. The full state of the drone is thus given by $\mathbf{x}_f = [\mathbf{q}, {}^b\boldsymbol{\omega}, {}^0\mathbf{p}_{CoM}, {}^b\mathbf{v}_{CoM}]^T \in \mathbb{R}^{13}$ where \mathbf{q} gives the orientation quaternion of the drone, ${}^0\mathbf{p}_{CoM}$ is the position of the CoM, and ${}^b\mathbf{v}_{CoM}$ its velocity. A fully actuated point mass model with linear dynamics was used as the simple model (Fig. 4) with state $\mathbf{x}_s = [{}^0\mathbf{p}_{CoM}^T, {}^0\mathbf{v}_{CoM}^T]^T \in \mathbb{R}^6$. The input for the model is a single force vector in 3D.

To handle working with unit quaternions in the full model, a change of variables to minimal coordinates is employed where Cayley parameters are used to describe changes in orientation [26] at each iteration. Although Cayley parameters experience a singularity at a rotation of π radians, since DDP makes small changes to the trajectory at each iteration, the singularity can be effectively avoided, even in cases when the nominal trajectory itself makes full rotations. The interested reader is referred to [26] for detail.

IV. SIMULATION RESULTS

In this section, we benchmark the MHPC performance via simulation on robots discussed in Section III. The MHPC performance is evaluated in terms of disturbance rejection for the quadruped and biped, and in terms of cost reduction for the quadrotor. Computational cost is benchmarked on each system for various abstraction schedules.

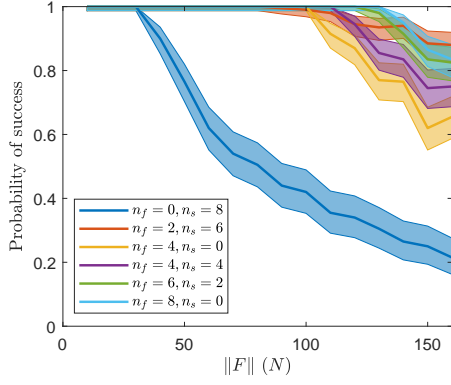
A. Quadruped

We use a 2D model of the MIT Mini Cheetah [27] as the quadruped testbed. MHPC is configured such that it replans each gait mode. Six different abstraction schedules are considered over this horizon. The quadruped executes bounding for four gait cycles, resulting in 16 modes in total.

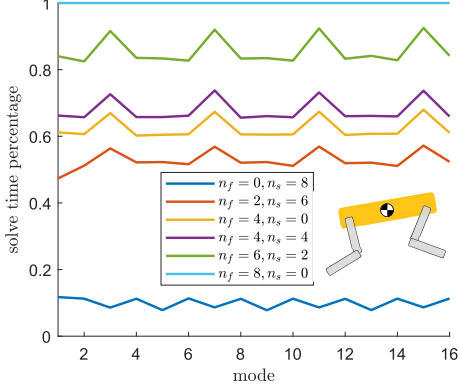
The time steps for dynamic simulation and MHPC are both 1 ms. The front-stance mode and the flight mode each run for 72 ms, and the back-stance mode runs for 80 ms. In Fig. 2, the overall planning horizon, the full-model horizon and the simple-model horizon are denoted t_{h_o} , t_{h_f} and t_{h_s} , respectively, for general representation. Here in this section, we denote them as n_o , n_f , and n_s , since they are counted as multiples of gait modes. Note that $n_o = n_f + n_s$. We consider $n_o = 8$ for five abstraction schedules, and vary n_f in the set $\{0, 2, 4, 6, 8\}$. The sixth schedule uses $n_o = n_f = 4$. In the rest of this paper, we use $\text{MHPC}(n_f, n_s)$ to represent MHPC that is associated with the abstraction schedule n_f and n_s . When $n_f \neq 0$, at least 2 gait modes are assigned to the full model. Therefore, the control generated by MHPC is the joint actuation and is directly applied to the quadruped. However, when $n_f = 0$, the MHPC essentially degenerates to simple-model MPC. The resulting control is then the GRF as shown in Fig. 3(a). In this case, we use $\boldsymbol{\tau} = \mathbf{J}^T \mathbf{F}$ to generate the joint actuation for the stance leg, and a swing foot controller as in [3] for the swing leg. A heuristic controller used by [18] is employed to warm start the full-model plan, and the simple-model plan is initialized with zeros. For each optimization, both the outer loop and inner loop of HSDDP are terminated at maximum of 3 iterations.

A push disturbance is applied on the trunk in the second flight for 30 ms. The magnitude of disturbance is increased from 10 N to 160 N. For each fixed magnitude, we estimate the probability of success by counting the number of successes out of 200 random trials. In each trial, the location and direction of disturbance are randomly generated according to a uniform distribution. A trial is considered a success in rejecting a disturbance if none of the following occur: self-collision, ground collision, and torque/joint limit violation.

Figure 5a statistically quantifies the robustness of MHPC for six abstraction schedules. The solid curves represent the estimated probability of success, around which the strip indicates a 95% confidence interval [28]. The top right corner indicates higher possibility of rejecting larger disturbances, whereas the left bottom corner indicates more likely failure for small disturbances. The configuration $\text{MHPC}(0,8)$ (simple-model MPC) has the worst performance, since it starts to fail at disturbances of 30 N. The configuration $\text{MHPC}(8,0)$ (whole-body MPC) has the best robustness, since it can reject disturbances as much as 130 N. The performance of other abstraction schedules lies in the middle between $\text{MHPC}(0,8)$ and $\text{MHPC}(8,0)$, demonstrating that incorporating full model planning would increase the robustness. The result of $\text{MHPC}(2,6)$ shows that even assigning a small amount of horizon to the full model could significantly improve the controller's robustness. Comparison between



(a) Robustness evaluation of MHPC for 6 abstraction schedules.



(b) Computation times of MHPC for 6 abstraction schedules.

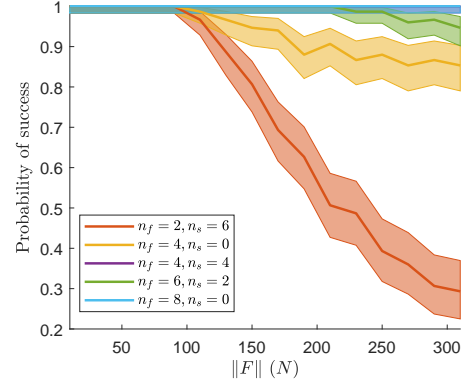
Fig. 5: MHPC performance obtained by quadruped bounding.

MHPC(4,4) and MHPC(4,0) reveals that the controller is improved by extending the horizon with the simple model. In this sense, both adding whole-body planning to a simple-model scheme, and adding simple-model planning to a whole-body scheme offer performance benefits.

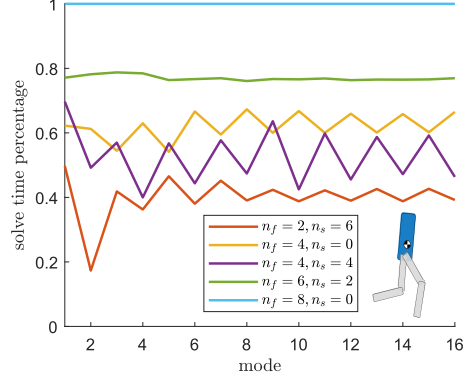
Figure 5b evaluates the computation time for six abstraction schedules, obtained assuming no disturbances. Sixteen computation times are acquired for each schedule since the simulation runs for 16 gait modes and the re-optimization occurs every one gait mode. The actual computation times are normalized over that of MHPC(8,0) (whole-body MPC). Unsurprisingly, the MHPC(0,8) (simple-model MPC) achieves the lowest computation time, whereas MHPC(8,0) has the highest, and the computation times of other MHPC schemes increases with n_f . This is because the full model has the highest-dimensional state space, and the computational complexity of DDP iterations are cubic in the dimension of the state space. Note that MHPC(2,6) achieves performance as good as whole-body MPC, while its computation efficiency is the second best. We conclude that with proper schedule, MHPC could achieve high performance rivaling whole-body MPC, while significantly lowering computational cost.

B. Biped

The biped testbed used in this work is the simulated robot Ernie [29] at the University of Notre Dame. MHPC is applied for four gait cycles with a target running speed of 1.5 m/s. The stance modes and the flight modes run for 110 ms and



(a) Robustness evaluation of MHPC for 5 abstraction schedules. MHPC(4,4), in purple, has the same probability of success as MHPC(8,0), in blue, for this case.



(b) Computation times of MHPC for 5 abstraction schedules.

Fig. 6: MHPC performance for control of biped running.

80 ms, respectively. The outer loop and inner loop of DDP are terminated at maximum of 3 and 15 iterations, respectively. All other simulation parameters (e.g., simulation and MHPC time steps, and overall planning horizon) are identical to the quadruped simulation in Section IV-A, and the same random tests are conducted for robustness evaluation.

Figure 6a depicts the probability of success of MHPC for 5 abstraction schedules in response to disturbances 0-320 N. The MHPC(0,8) (trunk MPC), is not shown here since the authors were unable to obtain a stable running gait for the biped with this approach. This finding is attributed to the fact that the balance problem for a biped is typically more difficult than that for a quadruped, and more whole-body details need to be considered in designing a stabilizing controller. As for quadrupeds, Figure 6a demonstrates that introducing the full model in the planning significantly improves the controller's robustness. Figure 6b depicts the computation times, where MHPC(4,4) takes less time than MHPC(4,0) to compute optimal solutions. This is because MHPC(4,4) takes less DDP iterations to converge. Surprisingly, MHPC(4,4) has the same probability of success as the whole-body MPC. Based on these observations, MHPC(4,4) is the preferred abstraction schedule for biped running in this case.

C. Quadrotor

To benchmark MHPC on quadrotor, a point-to-point trajectory is planned and executed (Fig. 7). The goal state is placed statically. MHPC is solved in a receding horizon fashion and

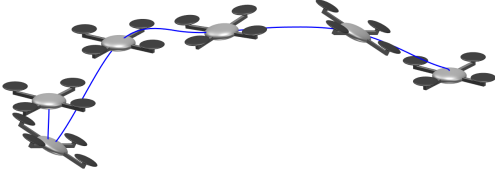


Fig. 7: Quadrator tests planned point-to-point motions from a starting configuration (left) to a goal configuration (right).

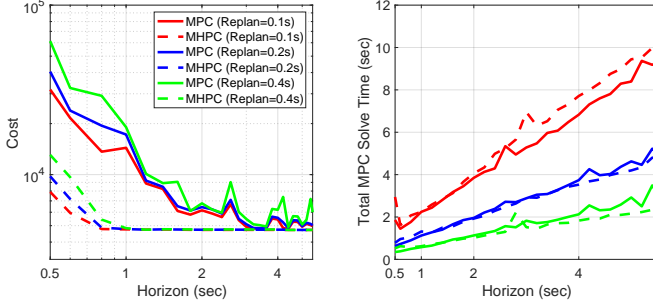


Fig. 8: Quadrator results comparing conventional MPC vs. MHPC.

the entire simulation lasts 10 s with a 0.02 s time step. The initial trajectory controls are all zeros for both models, so all controls of the system are generated by the solver. The running cost assigned to the full model is quadratic and includes a quaternion orientation term $(1 - (\mathbf{q}_d^\top \mathbf{q})^2)$. This cost is minimized at either the desired quaternion \mathbf{q}_d or its antipode $-\mathbf{q}_d$, which provides the same orientation. While running standard MPC, the terminal cost is set as the running cost scaled by 1000. When running MHPC, this terminal cost is added with the value function obtained from the infinite-horizon LQR for the simple model. To compare the two frameworks, the simulation was repeated varying the full-model prediction horizon and the re-planning rate. At each re-planning step, DDP is warm started using the previous plan and runs for a maximum of five iterations.

The total cost and the computation time are recorded along with each simulation. These results are plotted with respect to planning horizon in Fig. 8. Overall, the total cost decreases as the planning horizon is increased. However, the total cost of the MHPC stays steady once the planning horizon reaches 1 s, whereas this steady behaviour is observed at 3.2 s for standard MPC. In addition, the total cost changes more smoothly with planning horizon for the MHPC than for the MPC. Overall, MHPC results in solutions with lower and more reliable costs in shorter viable horizons for the full model. The result is as expected since, as discussed above, the terminal cost set for the full model by MHPC provides more insightful information to future motions whereas that by MPC is only heuristic.

V. 3D SIMULATOR AND EXPERIMENTAL VALIDATION

The proposed MHPC controller, specifically MHPC(2,6) as in Section IV-A, is implemented in the full 3D simulator developed for the MIT Mini Cheetah and on the Mini Cheetah Hardware [27]. The simulator is meant to mimic the robot hardware as closely as possible, with sensor noise

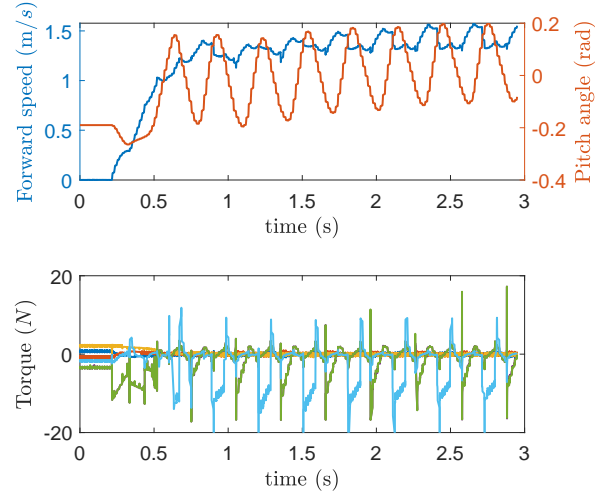


Fig. 9: Results from simulator during 1.5 m/s bounding. Top: forward speed and pitch angle. Bottom: hip and knee torques of front right and rear right legs.

corrupting state information from a state estimator. The control and estimation loops run at 1000 Hz in simulation and at 500 Hz on hardware.

The MHPC runs offline with time step 0.001 ms to generate an optimal control and trajectory for 8 gait cycles with target speed 1.5 m/s. The feed-forward part of this control policy is used directly as the joint actuation, whereas the feedback gain is scaled by 0.1 since actuator saturation were observed to occur otherwise in experiments. In addition, a PD-controller $\tau = -k_p(\mathbf{q}_{\text{joint}} - \mathbf{q}_{\text{joint},n}) - k_d(\dot{\mathbf{q}}_{\text{joint}} - \dot{\mathbf{q}}_{\text{joint},n})$ is employed to stabilize tracking where $k_p = 3(N \cdot m)/\text{rad}$ and $k_d = 1(N \cdot m)/\text{rad/s}$. Further, since the controller MHPC(2,6) discussed in Section IV-A is based on a planar quadruped, a roll controller as in [25] is employed to regulate roll in 3D.

Simulator data are shown in Fig. 9, where the forward speed, the pitch angle, and the hip and knee torques of the front right and back right legs are plotted. Since the robot starts with a static configuration with all feet on the ground, it takes around two gait cycles to transition to 1.5 m/s bounding. The same MHPC controller is also implemented on the hardware. Figure 10 shows time-series snapshots of Mini cheetah executing a bounding gait. In the experiment, the robot could bound up to 7 gait cycles. It fails in the subsequent gait cycles, largely because of the absence of a yaw controller and uncertainties from the state estimator. These issues will be addressed in future experiments. Online computation of the control policy would also improve the performance, and is the main focus for future work.

VI. CONCLUSIONS AND FUTURE WORKS

This work presented a novel Model Hierarchy Predictive Control (MHPC) architecture that combines the benefits of full-model MPC and simple-model MPC. The simple model is used in long-term planning to set a low-rank approximation of the optimal cost-to-go for the terminal cost of the full model. This approach automatically biases the full-model

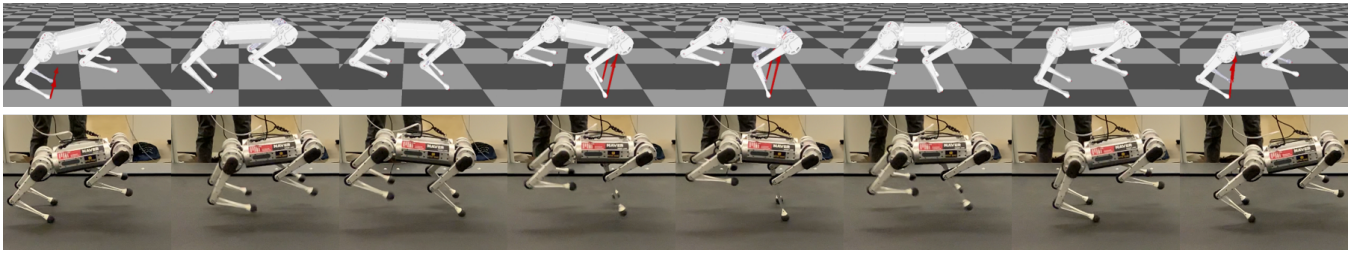


Fig. 10: Time-series snapshots of the robot executing a bounding gait. Top: Simulator motion capture. Bottom: Experiment motion capture.

optimization toward a favorable long-term plan as opposed to heuristic terminal costs authored into whole-body MPC. Further, the simple model has a low dimension and can reduce the overall computational cost. Employing a full model in near-term planning, even for a short period, is shown to significantly improve push robustness compared to MPC with a simple-model alone. Simulation results have shown that with proper abstraction schedule, MHPC could achieve high disturbance rejection performance comparable to whole-body MPC while maintaining significantly lower computational requirements.

Currently, the implementation of MHPC is computed offline and executed online. Future work will focus on online computation. Our preliminary work in this direction aims to provide a quadratically converging algorithm that efficiently computes needed partials by exploiting the structure of the dynamic equations of motion. Future work will also address the yaw control issue for the planar quadruped and unlock more dynamic behaviors by employing a 3D model.

REFERENCES

- [1] Y. Tassa, T. Erez, and E. Todorov, "Synthesis and stabilization of complex behaviors through online trajectory optimization," in *IEEE/RSJ Int. Conf. on Intelligent Robots and Systems*, 2012, pp. 4906–4913.
- [2] P.-B. Wieber, "Trajectory free linear model predictive control for stable walking in the presence of strong perturbations," in *IEEE-RAS Int. Conf. on Humanoid Robots*, 2006, pp. 137–142.
- [3] J. Di Carlo, P. M. Wensing, B. Katz, G. Bledt, and S. Kim, "Dynamic locomotion in the MIT Cheetah 3 through convex model-predictive control," in *IEEE/RSJ Int. Conf. on Intelligent Robots and Systems*, 2018, pp. 1–9.
- [4] T. Apgar, P. Clary, K. Green, A. Fern, and J. W. Hurst, "Fast online trajectory optimization for the bipedal robot Cassie," in *Robotics: Science and Systems*, 2018.
- [5] M. Neunert, M. Stuble, M. Gifftthaler, C. D. Bellicoso, J. Carius, C. Gehring, M. Hutter, and J. Buchli, "Whole-body nonlinear model predictive control through contacts for quadrupeds," *IEEE Robotics and Automation Letters*, vol. 3, no. 3, pp. 1458–1465, 2018.
- [6] C. D. Bellicoso, F. Jenelten, C. Gehring, and M. Hutter, "Dynamic locomotion through online nonlinear motion optimization for quadrupedal robots," *IEEE Robotics and Automation Letters*, vol. 3, no. 3, pp. 2261–2268, 2018.
- [7] P. M. Wensing and D. E. Orin, "High-speed humanoid running through control with a 3D-SLIP model," in *IEEE/RSJ Int. Conf. on Intelligent Robots and Systems*, 2013, pp. 5134–5140.
- [8] G. Bledt, P. M. Wensing, and S. Kim, "Policy-regularized model predictive control to stabilize diverse quadrupedal gaits for the mit cheetah," in *IEEE/RSJ International Conference on Intelligent Robots and Systems*, 2017, pp. 4102–4109.
- [9] A. W. Winkler, C. D. Bellicoso, M. Hutter, and J. Buchli, "Gait and trajectory optimization for legged systems through phase-based end-effector parameterization," *IEEE Robotics and Automation Letters*, vol. 3, no. 3, pp. 1560–1567, 2018.
- [10] D. E. Orin, A. Goswami, and S.-H. Lee, "Centroidal dynamics of a humanoid robot," *Auton. robots*, vol. 35, no. 2-3, pp. 161–176, 2013.
- [11] H. Dai, A. Valenzuela, and R. Tedrake, "Whole-body motion planning with centroidal dynamics and full kinematics," in *International Conference on Humanoid Robots*, 2014, pp. 295–302.
- [12] P. M. Wensing and D. E. Orin, "Generation of dynamic humanoid behaviors through task-space control with conic optimization," in *2013 IEEE International Conf. on Robotics and Automation*, 2013, pp. 3103–3109.
- [13] —, "Improved computation of the humanoid centroidal dynamics and application for whole-body control," *International Journal of Humanoid Robotics*, vol. 13, no. 01, p. 1550039, 2016.
- [14] S. Kuindersma, R. Deits, M. Fallon, A. Valenzuela, H. Dai, F. Permenter, T. Koolen, P. Marion, and R. Tedrake, "Optimization-based locomotion planning, estimation, and control design for the Atlas humanoid robot," *Auton. robots*, vol. 40, no. 3, pp. 429–455, 2016.
- [15] D. Mayne, "A second-order gradient method for determining optimal trajectories of non-linear discrete-time systems," *International Journal of Control*, vol. 3, no. 1, pp. 85–95, 1966.
- [16] R. Budhiraja, J. Carpentier, C. Mastalli, and N. Mansard, "Differential dynamic programming for multi-phase rigid contact dynamics," in *IEEE-RAS Int. Conf. on Humanoid Robots*, 2018, pp. 1–9.
- [17] C. Mastalli, R. Budhiraja, W. Merkt, G. Saurel, B. Hammoud, M. Naveau, J. Carpentier, L. Righetti, S. Vijayakumar, and N. Mansard, "Crocodyl: An efficient and versatile framework for multi-contact optimal control," in *Int. Conf. on Robotics and Automation*, 2020, pp. 2536–2542.
- [18] H. Li and P. M. Wensing, "Hybrid systems differential dynamic programming for whole-body motion planning of legged robots," *IEEE Robotics and Automation Letters*, vol. 5, no. 4, pp. 5448 – 5455, 2020.
- [19] J. Koenemann, A. Del Prete, Y. Tassa, E. Todorov, O. Stasse, M. Bennewitz, and N. Mansard, "Whole-body model-predictive control applied to the HRP-2 humanoid," in *IEEE/RSJ Int. Conf. on Intelligent Robots and Systems*, 2015, pp. 3346–3351.
- [20] E. R. Westervelt, J. W. Grizzle, and D. E. Koditschek, "Hybrid zero dynamics of planar biped walkers," *IEEE transactions on automatic control*, vol. 48, no. 1, pp. 42–56, 2003.
- [21] G. Lantoin and R. P. Russell, "A hybrid differential dynamic programming algorithm for constrained optimal control problems. part 1: theory," *Journal of Optimization Theory and Applications*, vol. 154, no. 2, pp. 382–417, 2012.
- [22] T. A. Howell, B. E. Jackson, and Z. Manchester, "ALTRO: a fast solver for constrained trajectory optimization," in *IEEE/RSJ Int. Conf. on Intelligent Robots and Systems*, 2019, pp. 7674–7679.
- [23] J. Hauser and A. Saccon, "A barrier function method for the optimization of trajectory functionals with constraints," in *IEEE Conf. on Decision and Control*, 2006, pp. 864–869.
- [24] A. Sherikov, D. Dimitrov, and P. Wieber, "Whole body motion controller with long-term balance constraints," in *2014 IEEE-RAS International Conference on Humanoid Robots*, 2014, pp. 444–450.
- [25] H.-W. Park, P. M. Wensing, and S. Kim, "High-speed bounding with the MIT cheetah 2: Control design and experiments," *The International Journal of Robotics Research*, vol. 36, no. 2, pp. 167–192, 2017.
- [26] B. Jackson and Z. Manchester, "Planning and control with attitude," in *Workshop on the Alg. Foundations of Robotics (submitted)*, 2020.
- [27] B. Katz, J. Di Carlo, and S. Kim, "Mini Cheetah: A platform for pushing the limits of dynamic quadruped control," in *IEEE Int. Conf. on Robotics and Automation*, 2019, pp. 6295–6301.
- [28] L. D. Brown, T. T. Cai, and A. DasGupta, "Interval estimation for a binomial proportion," *Statistical science*, pp. 101–117, 2001.
- [29] M. Fevre, B. Goodwine, and J. P. Schmiedeler, "Terrain-blind walking of planar underactuated bipeds via velocity decomposition-enhanced control," *The International Journal of Robotics Research*, vol. 38, no. 10-11, pp. 1307–1323, 2019.